JGR Oceans

RESEARCH ARTICLE
10.1029/2019JC015925

Relative Dispersion of Surface Drifters in the North Sea: The Effect of Tides on Mesoscale Diffusivity

Jens Meyerjürgens[1], Marcel Ricker[1], Vanessa Schakau[1], Thomas H. Badewien[1], and Emil V. Stanev[2]

[1]Institute for Chemistry and Biology of the Marine Environment, University of Oldenburg, Oldenburg, Germany, [2]Institute of Coastal Research, Helmholtz-Zentrum Geesthacht, Geesthacht, Germany

Key Points:
- Statistical Lagrangian metrics were derived from two clusters of surface drifters to analyze drifter dispersion in the North Sea
- Tracer stirring at the submesoscales is nonlocal and becomes local at the mesoscales
- Semidiurnal and shallow-water tides influence the relative diffusivities at the mesoscales

Correspondence to:
J. Meyerjürgens,
jens.meyerjuergens@uni-oldenburg.de

Citation:
Meyerjürgens, J., Ricker, M., Schakau, V., Badewien, T. H., & Stanev, E. V. (2020). Relative dispersion of surface drifters in the North Sea: The effect of tides on mesoscale diffusivity. *Journal of Geophysical Research: Oceans*, *125*, e2019JC015925. https://doi.org/10.1029/2019JC015925

Received 29 NOV 2019
Accepted 14 JUN 2020
Accepted article online 17 JUN 2020

Abstract We examine the relative dispersion and the contribution of tides on the relative diffusivities of surface drifters in the North Sea. The drifters are released in two clusters, yielding 43 pairs, in the vicinity of a tidal mixing front in the German Bight, which is located in the southeastern area of the North Sea. Both clusters indicate decreasing dispersion when crossing the tidal mixing front, followed by exponentially increasing dispersion with e-folding times of 0.5 days for Cluster 1 and 0.3 days for Cluster 2. A transition of the dispersion regimes is observed at scales of the order of the Rossby radius of deformation (10 km). After that, the relative dispersion grows with a power-law dependency with a short period of ballistic dispersion (quadratic growth), followed by a Richardson regime (cubic growth) in the final phase. Scale-dependent metrics such as the relative diffusivities are consistent with these findings, while the analysis of the finite-scale Lyapunov exponents (FSLEs) shows contradictory results for the submesoscales. In summary, the analysis of various statistical Lagrangian metrics suggests that tracer stirring at the submesoscales is nonlocal and becomes local at separation scales larger than 10 km. The analysis of meridional and zonal dispersion components indicates anisotropic dispersion at the submesoscales, which changes into isotropic dispersion on the mesoscales. Spectral analysis of the relative diffusivity gives evidence that semidiurnal and shallow-water tides influence relative diffusivity at the mesoscales, especially for drifter separations above 50 km.

Plain Language Summary The investigation of the transport and dispersal of biogeochemical substances and pollutants is of crucial importance for a broad spectrum of scientific research questions. To determine the risk of contaminants at the ocean's surface, numerical modeling frameworks are used for the prediction of tracer distribution on different spatial and temporal scales. Especially in tidally influenced shallow shelf seas, complex coastal processes hamper traditional particle modeling approaches, and observational data from surface drifters are required for calibration purposes. In this study, we estimate spreading rates from two clusters of surface drifters released in the southern North Sea, a shelf sea strongly affected by anthropogenic pressures. We provide the first estimate of spreading rates in this ecologically and industrially important area on different spatial and temporal scales. We further demonstrate from our drifter observations that tides influence diffusivity rates and provide a detailed analysis of tidal influence at different spatial scales.

1. Introduction

The oceanic flow field is turbulent over many spatial scales, which have an enormous impact on ocean circulation, heat transport, and stirring of tracers. Knowledge about the dispersal and pathways of tracers at the sea surface is crucial for a wide range of oceanographic research questions and provides valuable insights into the dispersal and fate of biological substances (Gawarkiewicz et al., 2007), pollutants (Maximenko et al., 2012; Poje et al., 2014), and climate-relevant tracers (Merlivat et al., 2015). The risk of anthropogenic pollutants and the impact of biogeochemical substances depend on the concentration of such materials at the ocean surface. However, understanding and prediction of these concentrations are of primary public and political interest. Several studies found a good agreement of simulated tracers and Lagrangian observations, but due to the limited amount of pairwise deployed drifters in the oceans (Beron-Vera & LaCasce, 2016; Romero et al., 2013), there is a significant lack of data coverage for many ocean areas (Meyerjürgens et al., 2019). Furthermore, more high-resolution Lagrangian data are needed to improve

the understanding of transition processes linking small-scale and submesoscale fluid dynamics and mesoscale ocean circulation. (Lumpkin et al., 2017; Özgökmen et al., 2012).

Lagrangian observations provide a direct method to sample the dynamics of a turbulent flow field in time and space and are required for the validation of Lagrangian particle tracking models. In recent decades, several studies derived statistical metrics from Lagrangian observations to characterize the properties of the underlying flow field (Koszalka et al., 2009; LaCasce & Ohlmann, 2003; van Sebille et al., 2015). For example, the mean square separation distance of particle pairs can be used to estimate the relative dispersion, which is a measure of the spreading of a particle cloud around its center of mass (Bennett, 2006; Koszalka et al., 2009; LaCasce, 2010; Ollitrault et al., 2005). The relative dispersion describes the mixing of passive tracers in a turbulent flow field and can provide information about the most important physical processes in the oceanic flow. Another essential statistical metric for the quantification of the stirring of a turbulent flow field is the relative diffusivity, which is the rate of change of relative dispersion.

Experiments with satellite-tracked drifters to study the relative dispersion and diffusivity of particles were carried out in the world oceans, for instance, in the Southern Ocean (van Sebille et al., 2015), in the North Atlantic Ocean (Lumpkin & Elipot, 2010; Ollitrault et al., 2005), in the South Atlantic (Berti et al., 2011; Dräger-Dietel et al., 2018), in the Gulf of Mexico (Beron-Vera & LaCasce, 2016; LaCasce & Ohlmann, 2003; Poje et al., 2014; Sansón et al., 2017), the Mediterranean Sea (Haza et al., 2007; Lacorata et al., 2001), and in the Nordic Seas (Koszalka et al., 2009). Other studies aimed at describing the dispersion of particle clouds in coastal areas, in surf zones, and in tidal inlets (Schroeder et al., 2012; Spydell et al., 2007, 2015). A recent study summarizes dispersion properties, derived from the Global Drifter Program data set, in different ocean basins worldwide and has pointed out that dispersion rates at the submesoscales are about 1 order of magnitude higher than at the mesoscale ranges (Corrado et al., 2017). The submesoscale, that ranges from hundreds of meters to tens of kilometers and at temporal scales from hours to days (McWilliams, 2016), connects the geostrophic mesoscale regime and the turbulent motion, in which vertical and horizontal mixing is linked and has a substantial contribution to the biogeochemical cycle in the ocean (Klein & Lapeyre, 2009; Lévy et al., 2012).

Lagrangian observations from drifter pairs have shown that submesoscale dispersion, with initial pair separation of ~5 to 100 m, increases roughly exponentially (Beron-Vera & LaCasce, 2016; Ohlmann et al., 2012). The exponential growth of the relative dispersion of particles indicates a nonlocal dispersion regime, in which eddies with scales larger than the separation of the particles contribute to the diffusivity. On the contrary, other studies reported local dispersion at the submesoscales, which means that the diffusivity is controlled by eddies of the same size as the particle separation (Poje et al., 2014; Schroeder et al., 2012).

Drifter deployments in the vicinity of horizontal fronts indicate converging zones in the submesoscales, which can result in a clustering of drifters and the concentration of flotsam at the ocean's surface (D'Asaro et al., 2018; Drinkwater & Loder, 2001; Poje et al., 2017; Schroeder et al., 2012). The numerical representation of dispersion and diffusivities in the coastal ocean is challenging because tides and turbulence induced by a complex bathymetry and estuarine processes hamper traditional approaches. Tides and small-scale estuarine processes in particular often have a massive impact on coastal ocean circulation (Delandmeter et al., 2017; Stanev et al., 2016), so understanding their implications on dispersal is of general interest, especially for pollutants entering the open ocean from land sources and rivers. Barotropic and baroclinic tides contribute to the horizontal ocean mixing and the baroclinic tides enhance substantially the vertical mixing (Stanev & Ricker, 2020; Suanda et al., 2017).

The amount of numerical studies of dispersion which have taken into account tides is limited. The studies which have incorporated baroclinic (Callies et al., 2019; Lynge et al., 2010; Suanda et al., 2018) and barotropic (Orre et al., 2006) tides analyzed dispersion processes in the submesoscales for several hours or days. Suanda et al. (2018), for instance, used numerical drifters to show that the inclusion of baroclinic tides in the model induces a 3–4 times larger horizontal diffusivity than barotropic tides in the submesoscales. Numerical experiments on the European Northwest Shelf demonstrated that barotropic tides massively influence the energy cascades on the mesoscales and increases the length of Lagrangian particle trajectories significantly (Stanev & Ricker, 2020). However, Lagrangian observations in the tidally influenced coastal ocean are still limited. Consequently, there is a considerable need for observational data to gain further

insight into the contribution of tides to diffusivities on the mesoscales to compare the results with the findings of the particle tracking models.

The purpose of this study is to analyze the submesoscale and mesoscale dynamics derived from two clusters of drifters in the North Sea. Semidiurnal tides, density gradients, and wind forcing dominate the circulation in the North Sea (Becker et al., 1992; Otto et al., 1990). We focus on the impact of tides and tidal mixing fronts on the dispersion aiming at advancing the understanding of processes influencing the fate and dispersion of particles at the ocean's surface (Christensen et al., 2018; Critchell et al., 2015). The investigation of this thin near-surface layer is crucial for the investigation of the fate of pollutants such as oil and floating plastics, which are mainly transported in this layer (Laxague et al., 2018).

We analyze the dispersion of drifters using traditional techniques of two-particle pair statistics and continue to focus on the effects of strong tidal dynamics on dispersion rates. The study is structured as follows. A brief description of the study site, the experiment, and the dispersion metrics is provided in section 2. The results of the dispersion metrics and the tidal analysis are presented in section 3. A discussion of the dispersion metrics focusing on the contribution of tides to the dispersion is given in section 4. A brief summary and conclusion of the results and the key messages of this study are provided in section 5.

2. Material and Methods

2.1. Study Site

The North Sea is a semienclosed shelf sea that opens into the Norwegian Sea in the north and into the English Channel in the west. The German Bight is located in the southeastern part of the North Sea and is one of the best observed coastal areas in the world based on Eulerian measurements (Baschek et al., 2017; Stanev et al., 2016). It is one of the most intensively used coastal areas worldwide and connects the English Channel with the major ports of Europe. As a result, the coastal region has great industrial and political importance for different stakeholders and is impacted by anthropogenic pressures. However, there is a significant lack of Lagrangian observations in this area (Meyerjürgens et al., 2019; Stanev et al., 2019).

The German Bight is a shallow-water shelf area and is profoundly impacted by semidiurnal tidal waves (M_2), and the residual circulation is cyclonic due to nonlinear tidal interaction and prevailing westerly winds (Becker et al., 1992; Huthnance, 1991; Otto et al., 1990). Baroclinic instabilities, wind forcing, and the gradient of the bottom topography can lead to the formation of eddies with spatial scales of several kilometers covering the transition zone between submesoscale and mesoscale dynamics (Badin et al., 2009; Becker et al., 1992). Freshwater runoff from the rivers Elbe and Weser in combination with oceanic water delivered by the English Channel form submesoscale filaments and mesoscale density fronts in the southeastern part of the German Bight (Becker et al., 1999; Dippner, 1993; Skov & Prins, 2001). Several studies reported high densities of floating material at these filaments and frontal systems in the German Bight (Gutow et al., 2018; Thiel et al., 2011).

2.2. Drifter Data

The data set analyzed in this study were derived from 14 satellite-tracked surface drifters forming 43 pairs, which were deployed in two clusters in the German Bight in October 2018. They sample the current in the upper 0.5 m of the water column and have four cruciform drag-producing vanes attached to the bottom of the housing to minimize the direct wind slip. The response of different drifter configurations to surface currents depends mainly on the ratio of the cross-sectional area of drifter components above and below the water surface (De Dominicis et al., 2016). This ratio is defined as the drag area ration (DAR). The DAR of this configuration is $R = 25.6$ (Meyerjürgens et al., 2019).

For the adequate resolution of submesoscale processes, the transmission interval for the position data was set to 10 min, which is transmitted directly via the Globalstar satellite telemetry. The drifter is powered by an external battery pack yielding an average battery lifetime of about 8 months by transmitting the position in near-real-time with an interval of 10 min, which provides a high signal-to-noise ratio. Positions of the drifters were tracked with an accuracy of ~2.5 m. The direct wind slip U_{slip} of the drifters is 0.27%, which would result in wind-induced velocities ranging from 0.0027–0.027 m s^{-1} by wind speeds in a range of 1–10 m s^{-1} (Meyerjürgens et al., 2019).

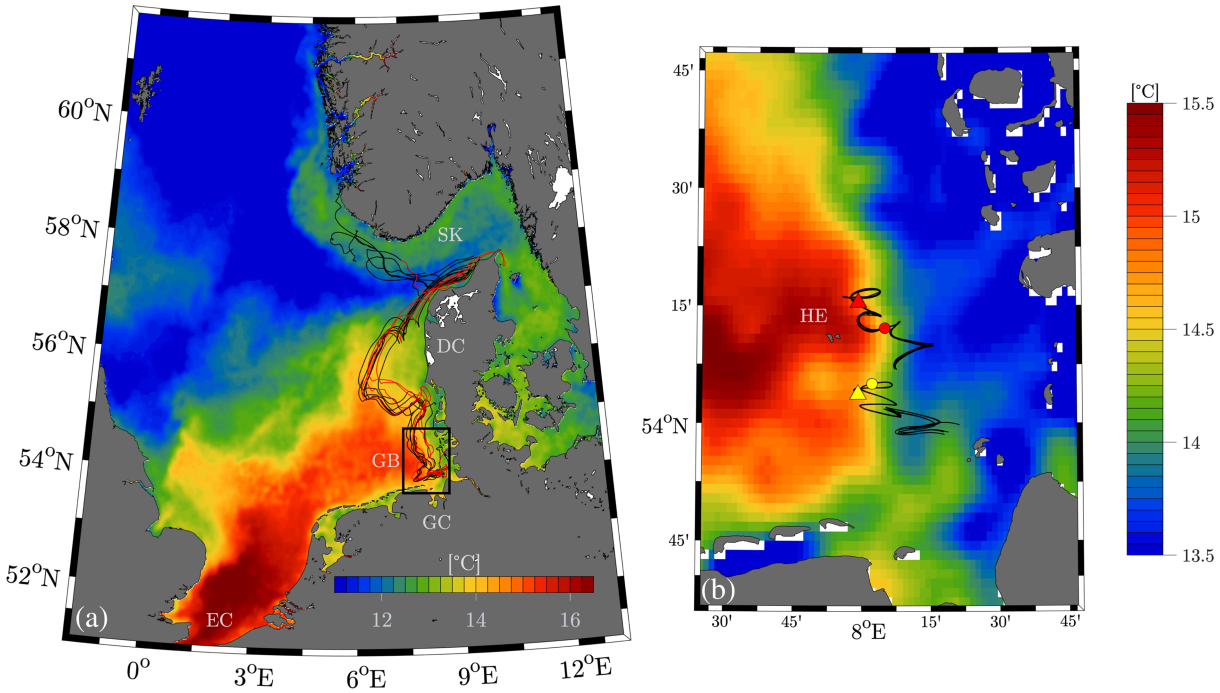

Figure 1. (a) Trajectories of 14 surface drifters (25-hr filtered data) deployed in two clusters (C_1 in black; C_2 in red) in the North Sea in October 2018. The drifters were released on 21 October in the German Bight with a cluster separation of 20 km. (b) Zoom of the deployment locations in the western area of the tidal mixing front. The deployment location of C_1 is marked with a red triangle, and the location of minimum dispersion is marked with a red circle. The deployment position and minimum dispersion location for C_2 are marked in yellow. Background colors are SST data on 21 October 2018 from Odyssea NW + IBI sea surface temperature analysis with a resolution of 0.02°. Acronyms: EC, English Channel; GC, German Coast; GB, German Bight; DC, Danish Coast; SK, Skagerrak; HE, Heligoland.

Outliers in the position data were excluded by applying a Hampel median filter for zonal and meridional coordinates separately with a window size of 18 surrounding samples (Lui et al., 2004). Samples that differ from the median by more than three standard deviations were excluded from the data set (amounting to less than 0.5% of the observations). The drifter positions were subsampled at a regular 10 min intervals using a piecewise cubic interpolation method (Fritsch & Carlson, 1980).

To compare the results of the Lagrangian metrics to other studies in other ocean basins where tides and inertial oscillations are typically suppressed by trajectory filtering, we also filtered the trajectories with a 25-hr Butterworth filter. That allows us to directly compare the results of the relative dispersion, relative diffusivity, and finite-scale Lyapunov exponents (FSLEs) with other studies. Further analyses, focusing on tidal effects on drifter velocities and relative diffusivities, were done with the unfiltered position data.

2.3. Drifter Deployments

Two clusters of drifters were deployed from the RV Heincke on 21 October 2018 in the German Bight close to a tidal mixing front. The front was identified by using near-real-time sea surface temperature (SST) satellite data from the Copernicus Marine and Environment Monitoring Service (CMEMS-SST-PUM-010-010-025). The horizontal resolution of the data is 0.02°, and data with processing Level 4 was used (Figure 1). The front was identified in the southeastern area of the German Bight in the vicinity of the island Heligoland. Both clusters were deployed in the western part of the front due to the local wind conditions with moderate westerly winds (Figure 1). The aim of the deployment strategy was that the drifters of both clusters cross the frontal system.

The drifters were deployed from the stern of the ship while the engines were stopped to ensure the least possible impact of the ship on the initial drift propagation.

Cluster 1 (C_1) consisted of eight drifters and was deployed on 21 October 2018 in the northeastern area of Heligoland. Another six drifters were released in a cluster (C_2) 2 hr later in the southeastern area of

Heligoland approximately 20 km away from the deployment location of C_1. The drifters were deployed with a maximum initial separation of 10 m.

The drifters were released in two clusters to increase the number of drifter pairs for a statistically valid analysis of pair separations. C_1 forms 28 pairs, and C_2 can be combined to 15 pairs. Drifter lifetime is affected by battery lifetimes, beaching of drifters, and oceanic conditions. For a statistically valid analysis, we used a minimum number of 10 pairs for the analyses of the Lagrangian statistics. As a result, we focused on the first 72 days for C_1 and the first 49 days for C_2. Trajectories of both clusters are shown in Figure 1.

2.4. Relative Dispersion

The relative dispersion ($D^2(t)$), which is a benchmark of the mean square separation of particle pairs, is defined by

$$\left\langle D^2(t)\right\rangle = \frac{1}{N}\sum_{i,j}\left[x_i(t)-x_j(t)\right]^2 + \left[y_i(t)-y_j(t)\right]^2, \tag{1}$$

where i and j refer to each drifter of a pair in the cluster of N drifter pairs and $x_{i,\,j}(t)$, $y_{i,\,j}(t)$ correspond to the coordinates in the Universal Transverse Mercator (UTM) projection at the time t. Typically, pairs or clusters of drifters that are initially separated by a small distance δ and were deployed at a certain time t_0 are used for the analysis. Various studies used "chance pairs," which are deployed randomly but are simultaneously present in a given study area, to increase the number of drifter pairs for Lagrangian statistics (Dräger-Dietel et al., 2018; LaCasce, 2010; Lumpkin & Elipot, 2010; Ollitrault et al., 2005; van Sebille et al., 2015). We have avoided the use of chance pairs in this study to overcome the issue of biased dispersion rates that can be produced for submesoscale dispersion (LaCasce & Ohlmann, 2003; Lumpkin & Elipot, 2010).

The rate of change of the relative dispersion characterizes the mixing properties of the flow field as a function of the length scales. It depends on the relative separation of a particle pair and is linked to the relative diffusivity (K):

$$K = \frac{1}{4}\frac{d}{dt}\left\langle D^2(t)\right\rangle. \tag{2}$$

Generally, four typical dispersion regimes can be distinguished, which depend on the time t and the averaged separation distance D between the drifter pairs, which are driven by the kinetic energy of the flow field. Richardson (1926) introduced the study of pair dispersion in the turbulent flow field of the atmospheric boundary layer. The Richardson regime is characterized by a dispersion following $D^2(t)\sim t^3$, which is mainly driven by processes with spatial scales similar to the drifter separation. Another regime which is related to local dispersion effects is the ballistic regime characterized by $D^2(t)\sim t^2$ with a squared growing behavior. Diffusive dispersion regimes are defined by a linear growth of relative dispersion in time. Regimes in which dispersion is driven by processes larger than the separation distance of the drifters are nonlocal showing an exponential growth of the dispersion in time:

$$\left\langle D^2(t)\right\rangle = \left\langle D^2(0)\right\rangle e^{\frac{t}{\tau}}, \tag{3}$$

where τ is the unfolding time that is related to the strain rate (Badin et al. 2011; Dräger-Dietel et al. 2018; Koszalka et al. 2009).

Equivalent scaling laws can be held for the relative diffusivity. We expect $K \propto D^{\frac{n+1}{2}}$ with spectral slopes of $n \leq 3$ for local dispersion and $n > 3$ for nonlocal dispersion effects (Bennett, 2006; LaCasce, 2010; Richardson, 1926).

2.5. Finite-Scale Lyapunov Exponents

A major drawback of relative dispersion is that this parameter characterizes the distribution of tracers at a given time and does not provide information on the dependence on spatial scales. To address this problem, we discuss further scale-dependent spreading properties of a flow field in the form of the FSLE.

Considering the relative dispersion alone may lead to inaccuracies caused by averaging all pair separations at fixed times. For example, averaging a pair with a distance of 1 km at a given time with a pair which is separated by 10 km may result in errors of an order of magnitude larger than the separation of the pairs. An alternative approach to describe the mixing properties of a flow field from a different perspective is a fixed-scale analysis by calculating the FSLE. Furthermore, considering the FSLE is more suitable if the dispersion processes in the flow field are more scale dependent rather than time dependent (Cencini & Vulpiani, 2013). On the other hand, there are some disadvantages concerning FSLEs. At small separation scales, the FSLEs are very sensitive to temporal resolution, interpolation, and filtering of the position data, while interpolation and filter effects hardly distort the FSLE results at larger spatial scales (Haza et al., 2014; Lumpkin & Elipot, 2010).

Generally, the Lyapunov exponent describes the rate of divergence of adjacent trajectories and is often used for the identification of exponential pair separation (Artale et al., 1997; Aurell et al., 1997; Haller & Yuan, 2000).

The FSLE λ is defined as the exponential growth rate of drifter separation as a function of the initial drifter separation D. It is calculated from the averaged time $< \vartheta(D) >$ that is required for a pair to increase the initial separation by the factor r.

$$\lambda(D) = \frac{\ln(r)}{<\vartheta(D)>}. \tag{4}$$

When relative dispersion follows a $\left\langle D^2(t) \right\rangle \sim t^{\frac{2}{\beta}}$ scaling, then the scaling of the FSLE is defined as the follows:

$$\lambda(D) \sim D^{-\beta}, \tag{5}$$

where $\beta = 0$ for exponential regime, $\beta = 2/3$ for local dispersion (Richardson regime), $\beta = 1$ in the ballistic regime, and $\beta = 2$ in the diffusive regime.

As discussed in Haza et al. (2008), the interpretation of the FSLEs is susceptible to the choice of the parameter r. The minimum value of r is given by the temporal resolution of the trajectory positions, since the time required for particle pairs to separate from D_0 to rD_0 need to be longer than the temporal resolution of the trajectory positions.

It should be noted that the FSLE analysis may identify different dispersion regimes than the dispersion-versus-time analysis since the latter analyzes the separation of pairs based on time scales and the FSLEs provide a measure of dispersion based on spatial scales.

2.6. Tidal Analysis

The influence of tides in the German Bight can be seen in oscillations of the drifter trajectories (Figure 1b). In order to characterize the effects of tidal oscillations on drifter velocities, we have applied a fast Fourier transform (FFT) to decompose the unfiltered velocity time series of the individual drifters into their representative frequencies. We applied the FFTs separately to the drifter data in the southern area and northern area of the North Sea to compare the amplitudes of tidal velocity in different regions of the North Sea. For analysis of the southern area, we considered the data of all drifters up to 55.5°N and, for the northern area analysis, the data of all drifters above 55.5°N. For comparison, we have applied the analysis to the entire data set. The results were averaged over all drifter trajectories. In addition, the tidal harmonic analysis toolbox (UTide) was used to study the influence of distinct tidal constituents on the oscillation amplitudes (Codiga, 2011).

The effects of tides on diffusivities at the submesoscales were addressed by several studies (Orre et al., 2006; Spydell et al., 2015; Suanda et al., 2018). However, the implications on the mesoscales remain unclear, as well as the contributions of different tidal constituents to the diffusivities.

To close this gap, we analyzed the effects of different tidal constituents on the relative diffusivities of the drifter pairs. Since the relative diffusivity is a scale-dependent measure, we investigated the contribution of tides on the relative diffusivity on different separation scales. Therefore, we decomposed the relative diffusivity of all drifter pairs into their respective frequencies using FFT. We applied this analysis to different maximum

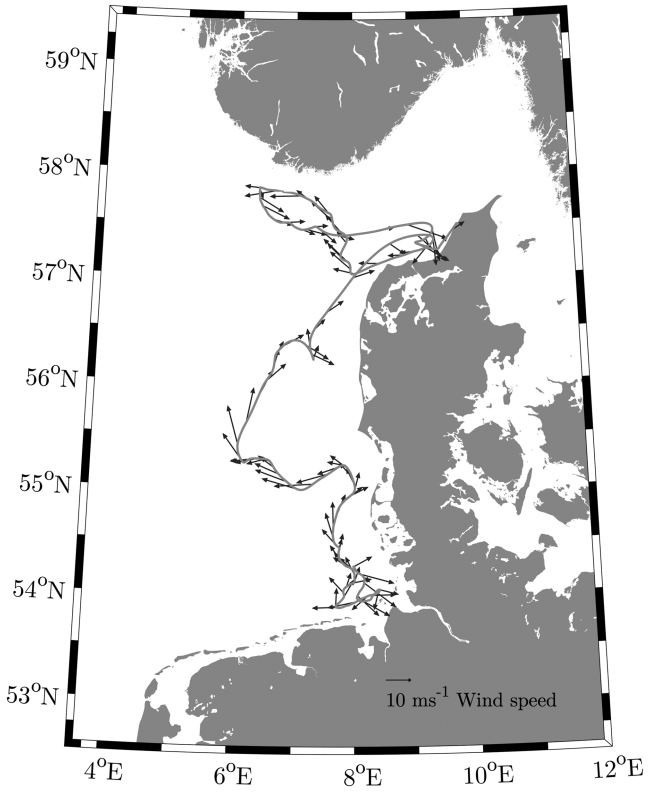

Figure 2. Wind data, interpolated to a drifter trajectory from cluster C_1. Wind speeds and directions are indicated by black arrows every 18 hr. The drifter trajectory is represented by a gray line.

drifter separations (D_{max}) in order to gain insight into the contribution of tides at different separation scales. The results of the FFTs were averaged for the different maximum pair separations. We have chosen a minimal trajectory length of 4 days to obtain statistically significant results. The mean trajectory lengths are 7.9 days for D_{max} = 10 km, 24.5 days for D_{max} = 25 km, 35.3 days for D_{max} = 50 km, 40 days for D_{max} 75 km, 41.7 days for D_{max} = 100 km, and 44.3 days for D_{max} = 150 km.

2.7. Wind Effects

In order to get an impression of the wind influence on the pathways of drifters, we compared the drifter velocities to wind data from a numerical model of the German Weather Service (DWD). The model has a spatial resolution of 7 and 3.5 km in meridional and zonal direction, respectively. The temporal resolution is hourly. The wind data were interpolated in space and time to the positions of a single drifter, which represents the general propagation of both clusters well. The drifter velocities were computed by taking the temporal derivations of the drifter positions. In order to eliminate short-term variations, both wind and drifter velocities were filtered with a moving average at a window length of 24 hr. The comparison of wind and drifter vectors show a good agreement (Figure 2). The maximum wind speeds observed in this study were 16.25 and 15.23 m s^{-1} for the zonal and meridional components, respectively.

3. Results

3.1. Relative Dispersion

The relative dispersion calculated from clusters C_1 and C_2 with an average initial separation of $D_0 \approx 10$ m is shown in Figure 3 with a 95% confidence interval for the averaged relative dispersion. The fitting parameters and the corresponding errors are determined by least squares. The initial growth phase of the relative dispersion for C_1 in the first 5 days shows an exponential growth rate of 2 ± 0.11, corresponding to an e-folding time of 0.5 ± 0.09 days for separation scales less than 10 km and time scales smaller than 5.5 days. As mentioned in section 2.4, the exponential growth of the relative dispersion indicates a nonlocal dispersion regime in which the dispersion is driven by mesoscale velocity field characteristics much larger than the separation scales. It should be noted that the relative dispersion increases for the first 0.8 days very slowly and decreases from 0.8 days to 1.5 days from 0.043 to 0.014 km^2 in the center of the salinity front, which indicates convergence of the drifters during this period (Figures 1b and 3a).

C_2 shows a slowly decreasing relative dispersion for time scales up to 0.6 days from an initial average dispersion of 0.056 to 0.026 km^2 (Figure 3c). As observed for C_1, the minimum value of the averaged relative dispersion is reached at the center of the tidal mixing front (Figure 1b). From 0.6 to 3.3 days and separation scales up to 10 km, the relative dispersion increases exponentially in time with a growth rate of 3.3 ± 0.14, which corresponds to an e-folding time of 0.3 ± 0.05 days. In this phase, the relative dispersion is also dominated by processes much larger than the drifter separation, which indicates a nonlocal dispersion regime.

After this initial phase, the relative dispersion of both clusters follow a power-law dependency in the scaling of

$$< D^2 > \propto t^n. \tag{6}$$

C_1 shows a short period of decreasing dispersion, which is followed by a period of strong increase. Overall, this intermediate period between 5.5 and 12 days can best be described by the theoretical prediction of the ballistic regime with a t^2 scaling (estimated slope $t = 2.1 \pm 0.3$), where the dispersion is mainly driven by the local shear of the velocity field. For times larger than 12 days, the dispersion of the estimated slope of

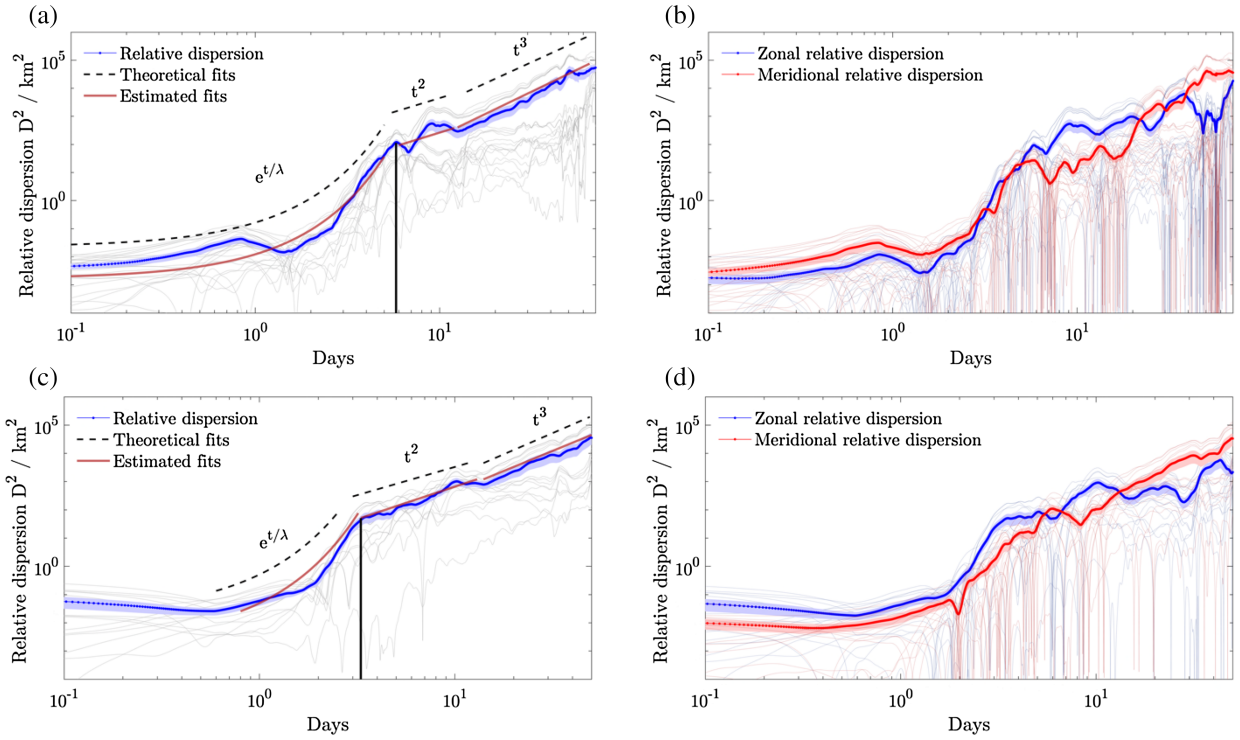

Figure 3. Relative dispersion from filtered position data versus time plot on a log–log scale. (a) Relative dispersion of C_1 and (c) for C_2. The average over all pairs is shown by the blue line, and the relative dispersion of the individual pairs is indicated by thin gray lines. The estimated fits are shown as solid red lines, and the theoretical fits are shown as black solid lines. The vertical solid line represents the regime transition of relative dispersion. (b) Relative dispersion of zonal (blue line) and meridional (red line) dispersion for C_1 and (d) for C_2. Solid lines indicate the average over all pairs, and thin lines show the relative dispersion of the individual pairs. The shading of all lines indicate the 95% confidence intervals.

the fit is $t = 3.1 \pm 0.1$ and follows the theoretical prediction by Richardson and scales as t^3. The spreading of the drifters in this regime is mainly influenced by current characteristics of scales similar to the drifter separation.

The dispersion of C_2 indicates ballistic dispersion within the period of 3.3 to 12 days with an estimated slope of 2.3 ± 0.1. As observed for C_1, the intermediate period is followed by local dispersion in the form of a Richardson regime. The estimated slope of the fitted power function is 2.9 ± 0.1 for this period. The first regime transition for C_1 occurs at the integral time scale of 5.8 days, while C_2 represents a regime transition to the integral time span of 3.3 days (Figure 3c). The transition from ballistic to Richardson regime for both clusters takes place after 12 days on separation scales of about 30 km.

Figure 3 also displays the meridional and zonal relative dispersion with 95% confidence intervals separately. Both components are showing exponential growth in the initial separation phase, which is followed by an oscillating trend at the intermediate and final phases.

There is evidence for an isotropic velocity field in the submesoscales due to the homogenous increasing of the zonal and meridional dispersion with no significant differences. At intermediate scales, the zonal dispersion becomes slightly larger than meridional dispersion, indicating anisotropic dispersion. At large scales, dispersion is meridionally anisotropic for both clusters. The zonal dispersion of C_1 decreases significantly over the period of 38 to 48 days (Figure 3b). C_2 shows a decrease in zonal dispersion over a period of 43 to 50 days (Figure 3d). During these periods, the meridional dispersion shows a significant increase in both clusters.

3.2. Relative Diffusivity

The relative diffusivity is the time derivate of the relative dispersion, which depends on the pair separation D and describes the mixing properties of the flow field as a function of the spatial scales of the drifter separation. The relative diffusivity is plotted against the separation D at specific spatial scales. To achieve this, we

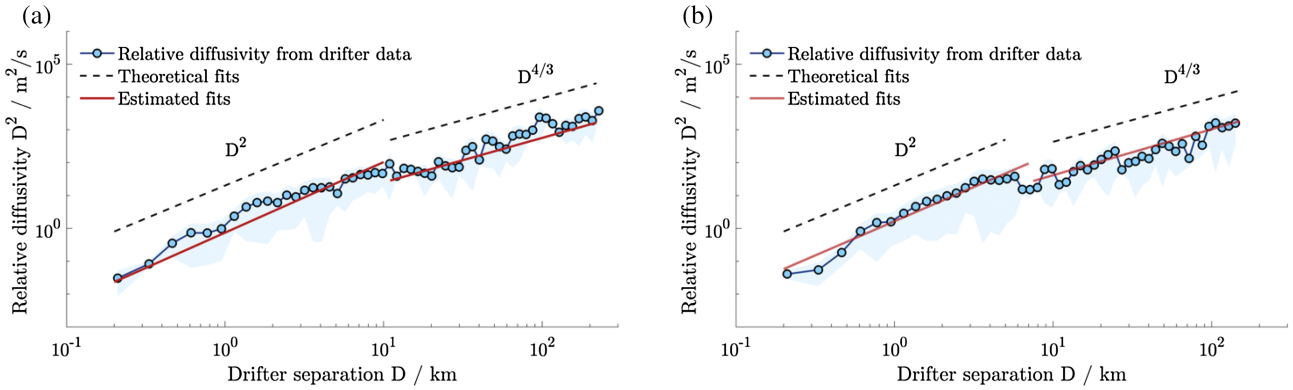

Figure 4. Relative diffusivity from filtered position data versus drifter separation plots on a log–log scale. The circles indicate the relative diffusivities averaged over certain distances, and the shaded line is the 95% confidence interval. The black dashed lines represent the theoretical fits and the red solid lines the estimated fits of relative diffusivity. Panel (a) shows the relative diffusivity for C_1 and panel (b) for C_2.

have averaged the diffusivity for all pairs at certain separation distances, according to Koszalka et al. (2009), with the dependence

$$D_n = \alpha D_{n-1} = \alpha^n D_0, \tag{7}$$

with $\alpha = 1.1$, which produces an exponential growth of the bin size with resulting nearly equally spaced bins on a logarithmic scale.

The relative diffusivity and the corresponding 95% confidence intervals of C_1 and C_2 are presented in Figure 4. The diffusivity of both clusters increases with the dependence $K \propto D^2$ for spatial scales smaller than 10 km, indicating nonlocal dispersion at these scales, which is in a good agreement with the dispersion analysis. The estimated slopes on these scales are 2.2 ± 0.2 and 2.1 ± 0.2 for C_1 and C_2, respectively. The diffusivity on larger spatial scales grows with calculated slopes of 1.3 ± 0.3 for C_1 and 1.4 ± 0.2 for C_2 according to a $D^{4/3}$ power-law, which corresponds to the theoretical prediction of Richardson, (1926) and indicates a local dispersion regime. Diffusivity magnitudes increase to values around 10^4 m^2 s^{-1}, which agrees with values in the Nordic Seas (Koszalka et al., 2009). The regime transition is clearly visible in both data sets at separation scales of approximately 10 km, which is close to the range of the Rossby deformation radius, which ranges from 5 to 20 km (Badin et al., 2009; Becker et al., 1999; Langenberg, 1998).

3.3. Finite-Scale Lyapunov Exponent

As discussed in section 2.5, we have analyzed the FSLEs for both clusters to shed light on the mixing properties from a fixed scale perspective. Previous studies discussed the choice of the parameter *r,* which must be a compromise between minimizing the noise of the fits and the resolution of the FSLEs at small separation scales (Haza et al., 2008; Lumpkin & Elipot, 2010; van Sebille et al., 2015). We used the parametrizations of an analysis of drifter pairs in the southern Pacific with a range of 1.15 to 2 (van Sebille et al., 2015) and added 1.4 for *r* used in a recent study in the South Atlantic (Dräger-Dietel et al., 2018). Figure 5a shows the FSLEs for C_1 plotted against the drifter separation.

Different values for the scale factor *r* are color-coded, and the solid lines show the theoretical prediction of the Richardson regime ($\lambda(D) \sim D^{-2/3}$) and the ballistic regime ($\lambda(D) \sim D^{-1}$). As in several other studies, different scaling regimes $\lambda(D) \sim D^{-\beta}$ are observed as a function of drifter separation (Dräger-Dietel et al., 2018; van Sebille et al., 2015). Furthermore, the regime transitions are clearly visible at separation scales of approximately 10 km, as observed in the relative diffusivity analysis. For separations from a few meters to 10 km, the scaling is $D^{-2/3}$, indicating local dispersion in the form of a Richardson regime. This is in contrast to the results of dispersion and diffusivity analysis, which show a nonlocal dispersion in the first observed dispersion regime. For separations from 10 to 300 km, the FSLE analysis identified the scaling D^{-1}, which refers to the ballistic regime. This is in line with the results of the dispersion analysis and agrees with the diffusivity analysis, which shows a Richardson regime on these scales. The results of the FSLEs of C_2 are shown in Figure 5b with the same color-coded values for *r* as for C_1. The observed scaling regime is consistent with

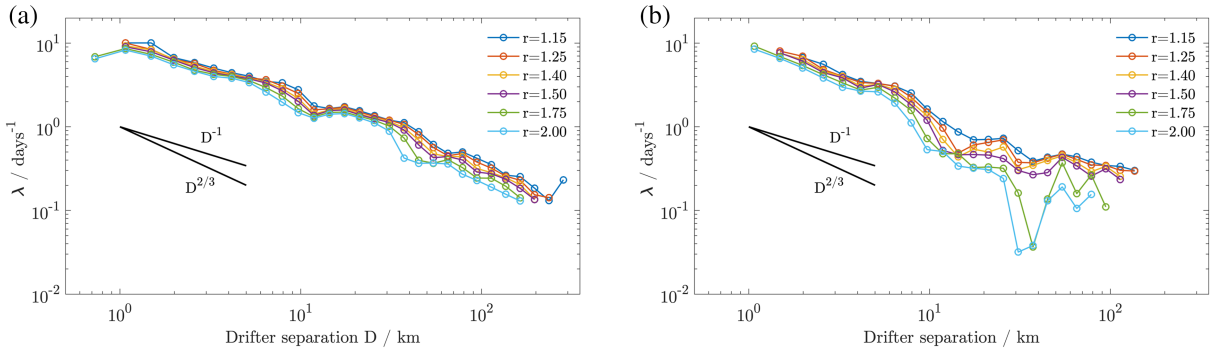

Figure 5. Finite-scale Lyapunov exponents from filtered position data for (a) C_1 and (b) C_2. The circles are mean values of the FSLEs of certain drifter separations. The colors refer to different values of the parameter r. The black lines indicate the theoretical prediction for the ballistic (D^{-1}) and Richardson ($D^{-2/3}$) regime.

the findings of C_1 indicating a Richardson regime for separation scales up to 10 km. For separations above 10 km, the FSLEs are strongly scattered, but for $r \leq 1.5$, there is evidence for a Richardson regime. There is no evidence for an exponential dispersion behavior in the FSLEs analysis that contradicts the dispersion results of both clusters. Due to the limited number of drifter pairs, the inaccuracies of the FSLEs on small scales are large. Of course, there are some discrepancies when comparing the results of the FSLEs to the results of the relative dispersion and diffusivity on the submesoscales, but regime transitions are detected in all analyses at 10 km in the range of the Rossby radius of deformation.

3.4. Tidal Analysis

As described in section 2.6, we have analyzed the influence of tides on the drifter velocities and the relative diffusivities derived from drifter pairs. Table 1 summarizes the results of the harmonic tidal analysis of zonal and meridional velocity components of the entire data set. The tidal amplitudes for the zonal velocity components are significantly higher compared to the meridional amplitudes.

For both components, the semidiurnal tidal components are significantly higher than the diurnal tidal components. Both analyses show peak values at the M_2 semidiurnal tidal constituent and also smaller peaks for shallow-water tidal constituents (M_4 and M_6) (Figure 6; Table 1).

The region-dependent analysis indicates that the amplitudes of the tidal currents in the southern area (<55.5° latitude) are significantly higher compared to the currents in the northern region (>55.5° latitude) of the North Sea (Figure 6). The FFT shows significant peaks for the M_2 constituent for the data of the southern area with higher velocities for the zonal component. The analysis of the northern region data indicates a small peak for the M_2 period with a velocity amplitude of 0.06 m s^{-1} in the meridional direction, while the zonal component shows no significant peak for the M_2 period. The velocity amplitudes for the southern region are significantly higher with values of 0.35 and 0.19 m s^{-1} for the zonal and meridional components, respectively. These results are consistent with previous studies in the region (Callies et al., 2019; Meyerjürgens et al., 2019; Port et al., 2011). The inertial period for the study area is computed from the average latitude for all drifters ($T_{inertial}$ = 14.57 hr) and does not show a peak in the FFT analysis.

Table 1
Results of the Harmonic Analysis of the Zonal and Meridional Velocities Averaged Over all Drifters With the Toolbox UTide

Tidal constituent	Period (hr)	Zonal velocity amplitude (m s^{-1})	Meridional velocity amplitude (m s^{-1})
M_2	12.421	0.205	0.113
S_2	12.000	0.065	0.035
N_2	12.658	0.041	0.021
M_4	6.210	0.023	0.008
NO_1	24.833	0.022	0.013
Q_1	26.868	0.021	0.010
M_6	4.140	0.009	0.003
M_8	3.105	0.002	0.002
O_1	25.819	0.007	0.013
MS_4	6.103	0.016	0.007

Note. The periods of the tidal constituents are expressed in hours, and the velocity amplitudes are expressed in m s^{-1}.

The spectral analysis of the relative diffusivities is shown in Figure 7. As described in section 2.6, we have used different maximum pair separations for the spectral analysis to investigate the influence of tides on the diffusivity on different spatial scales. The FFTs for the relative diffusivities do not show significant peaks for maximum separation distances below 25 km (Figure 7a). For D_{max} = 25 km, less pronounced peaks are indicated with diffusivity rates of about 50 m^2 s^{-1} for the M_2 semidiurnal constituent (Figure 7b). With increasing maximum pair separation, the peaks become more pronounced with increasing amplitudes, and also peaks

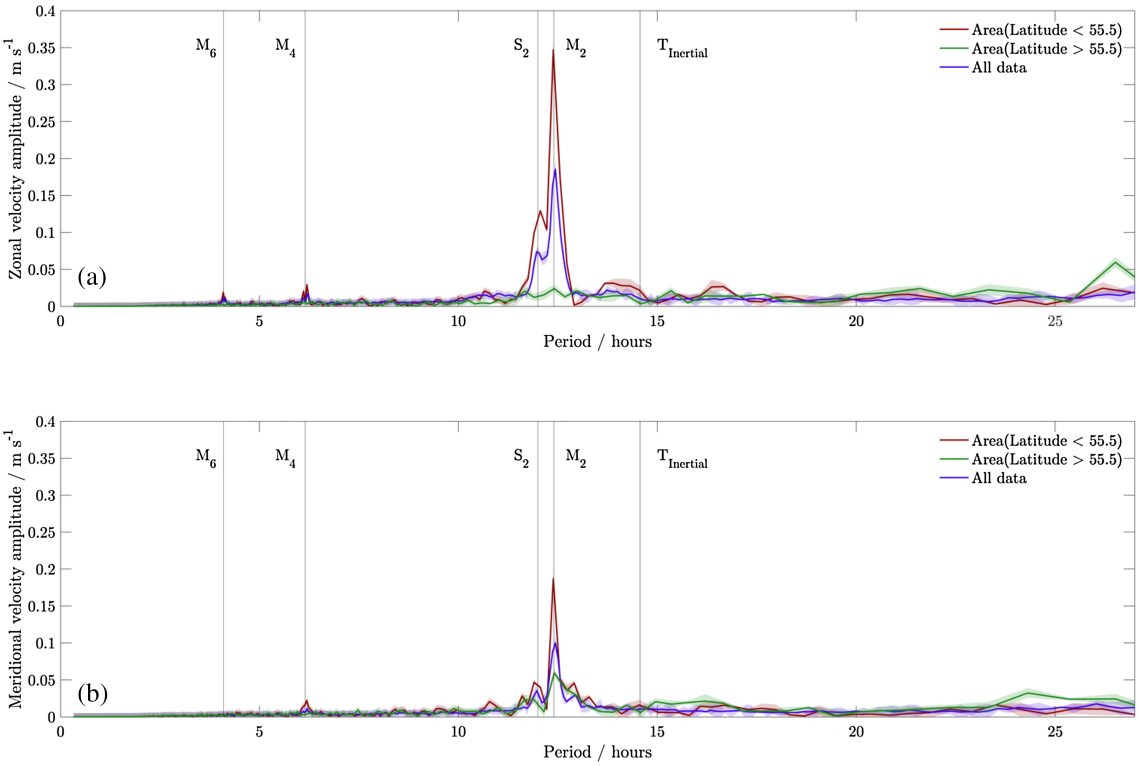

Figure 6. Spectral analysis of zonal (a) and meridional (b) drifter velocities, averaged over all drifters. The periods of the semidiurnal, shallow-water tidal components and the inertial period are marked by the vertical black lines, and the 95% confidence intervals are shown as shaded lines.

for shallow-water constituents are observed. For $D_{max} = 150$ (Figure 7f), the diffusivity amplitudes are about 4 times higher than the values for $D_{max} = 25$ km, with values around 200 m^2 s^{-1} for the M_2 semidiurnal tidal constituent and distinct peaks for shallow-water constituents (65 m^2 s^{-1} for M_4, 24.5 m^2 s^{-1} for M_6). Overall, the spectral analysis shows a diffusivity amplitude of 289.5 m^2 s^{-1} induced semidiurnal tides, which is comparable to diffusivities in the North Atlantic (Roach et al., 2018).

4. Discussion

We have analyzed the mixing characteristics in the eastern part of the North Sea with two-particle-pair-statistics methods derived from 43 drifter pairs, which were deployed in two clusters. The consideration of scale-dependent as well as time-dependent metrics provides a comprehensive overview of the dispersion properties in this area. Further, we investigated the contribution of tidal effects on different spatial scales to the relative diffusivities of the drifter pairs.

4.1. Two-Particle Pair Statistics

The dispersion of both clusters is significantly low in the vicinity of the baroclinic tidal mixing front and showing exponential increases while leaving the area of the front. One possible explanation for the decreasing dispersion is the convergence of velocity field along the density front, which results in the clustering of the drifters. Convergence could be enhanced by baroclinic mixing at tidal mixing fronts (Stanev, Al-Nadhairi, et al., 2015), but the vertical effects cannot be analyzed by surface drifter observations alone. However, several studies have observed declining dispersion rates, which are associated with horizontal convergence caused by density fronts at the submesoscales as well. Overall, there is evidence that convergence processes, induced by the tidal mixing front in the eastern German Bight, contribute to the clustering of drifters in our observations. These findings are consistent with studies which found high concentrations of floating materials in the area of the tidal mixing front in the southeastern part of the German Bight (Gutow et al., 2018; Thiel et al., 2011) and in other coastal regions in the world ocean (Acha et al., 2003; Hinojosa et al., 2010).

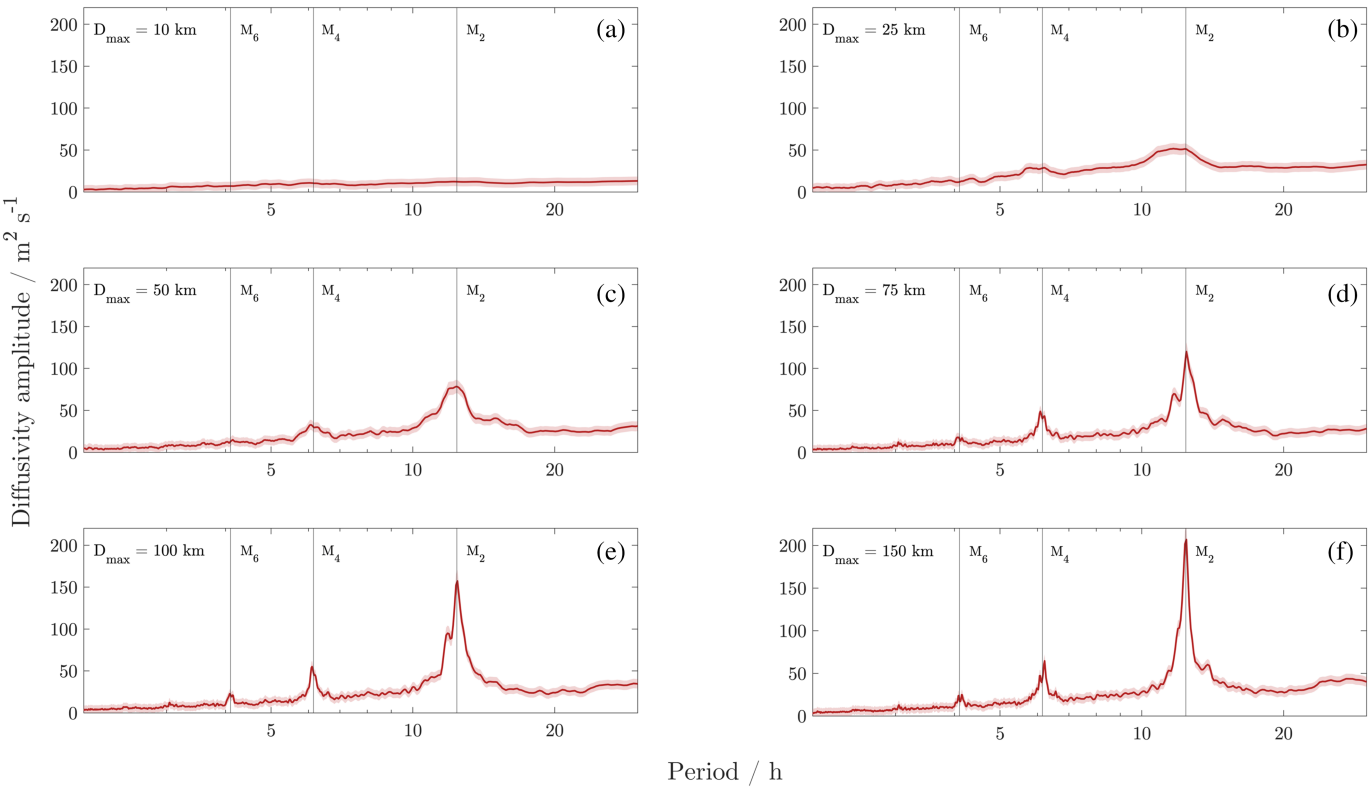

Figure 7. Spectral analysis of the relative diffusivities at certain maximal pair separations (D_{max}). The x axis displays the tidal period in hours and the y axis the diffusivity amplitude in $m^2\ s^{-1}$. Panel (a) shows the results for $D_{max} = 10$ km, panel (b) for $D_{max} = 25$ km, panel (c) for $D_{max} = 50$ km, panel (d) for $D_{max} = 75$ km, panel (e) for $D_{max} = 100$ km, and panel (f) for $D_{max} = 150$ km. The red line indicates the average of the spectral analysis results for all pairs with a maximum separation of D_{max}, and the shaded line is the 95% confidence interval. Semidiurnal and shallow-water tidal constituents are marked by black lines.

Our results suggest that coastal ocean models or regional models with fine resolution should more deeply address how well mesoscale and submesoscale processes, which massively impacts the dispersion and converging of tracers at the sea surface, are resolved. A crucial step in this direction is demonstrated in the comparative studies of Graham (2018) and Guihou et al. (2018).

The analysis of the relative dispersion shows an exponential growth for both clusters, which correspond to the results of the relative diffusivity indicating a squared growth for separation scales up to 10 km, which is in the order of the Rossby radius of deformation in the southern North Sea (Badin et al., 2009; Becker et al., 1999). In contrast, the FSLEs indicate a Richardson regime ($\lambda(D) \sim D^{-2/3}$) for both clusters at small scales. Discrepancies between different dispersion metrics have been reported in several other studies due to inertial motions and strong tidal oscillations that may contaminate the FSLEs at the submesoscales (Beron-Vera & LaCasce, 2016; Essink et al., 2019; van Sebille et al., 2015). In addition, disparities between the FSLEs and the relative dispersion can be caused by position uncertainties and sampling frequency of the drifters, which can significantly influence the results in the submesoscales (Haza et al., 2014). In order to minimize these effects, we used drifters with high sampling frequencies (10 min) and position uncertainties of approximate 2.5 m and carried out the deployment very carefully in order to minimize the impact of the ship on the initial cluster dispersion. However, we cannot completely rule out the possibility that our FSLE estimates are not contaminated due to the above-mentioned issues on the submesoscales.

Evidence of exponential regimes at the submesoscales for the relative dispersion and diffusivity is reported for many other ocean basins (Beron-Vera & LaCasce, 2016; Berti et al., 2011; Dräger-Dietel et al., 2018; Essink et al., 2019; van Sebille et al., 2015). The e-folding times derived from the dispersion analysis for C_1 is almost twice as high as for C_2. As a consequence, the relative dispersion for C_2 increases more quickly than the dispersion for C_1 and that the regime transition is reached for C_2 much faster. This could be the consequence of the different locations where the clusters were released. C_2 was deployed near the island of

Heligoland, where a complex, nonlinear interaction between tidal currents and bathymetry gradients could influence the dispersion. This effect was also observed by Tseng (2002), which found high dispersion rates induced by island wakes. The analysis of two individual clusters show that e-folding times of nearly simultaneously deployed groups of drifters can differ significantly due to complex coastal ocean processes.

The e-folding times observed in this study are significantly lower compared to other ocean basins, which means that the drifters separate much faster compared to other studies in the submesoscales (Beron-Vera & LaCasce, 2016; Essink et al., 2019; van Sebille et al., 2015). These results agree with a recent study in the German Bight, which mainly looked for submesoscale dispersion effects in the vicinity of offshore wind farms (Callies et al., 2019). Due to the limited length of the trajectory time series and the limited number of drifter pairs, the study only speculated that nonlocal dispersion occurs in the submesoscales in the German Bight. The authors further speculate that nonlocal dispersion was caused by the nonlinear effects of offshore wind farms. Our results confirm the observed nonlocal dispersion on the submesoscales, and the difference in the e-folding times suggests that nonlinear interaction with bathymetric gradients and island wakes has a significant impact on the dispersion rates.

Overall, the general findings of nonlocal dispersion in the submesoscales followed by a local dispersion regime at larger scales are consistent with previous studies (Corrado et al., 2017; Dräger-Dietel et al., 2018; Koszalka et al., 2009; LaCasce, 2010; van Sebille et al., 2015). However, diffusive regimes with linear dispersion scaling which were observed in multiple studies in the world oceans (Corrado et al., 2017; Dräger-Dietel et al., 2018; Koszalka et al., 2009) could not be identified in our analysis. This might be caused by boundary effects due to the finite length of the measurement. In a diffusive regime, the pair velocities are uncorrelated, and the scales of processes driving the dispersion of particles are larger than the pair separation. This leads to a diffuse dispersion at relatively large separation scales, which can hardly be achieved in the North Sea due to its semiclosed structure. This results in comparatively short residence times of the particles due to the high probability of getting trapped in coastal areas. Furthermore, the general transport pattern of the drifters is very strongly influenced by the wind conditions since the drifters are transported with the wind-driven surface currents (Figure 2). Wind forcing does not affect drifter dispersion because the wind influence on the drifters and the surface currents is quasi-simultaneous (Meyerjürgens et al., 2019; Poulain et al., 2009).

4.2. Zonal and Meridional Dispersion

The analysis of zonal and meridional dispersion shows an isotropic dispersion at the submesoscales but become anisotropic at intermediate scales, with higher magnitudes of zonal dispersion (Figures 3b and 3d). This might be due to the strong effects of tidal currents with tidal ellipses that are very pronounced in the zonal direction (Figure 6) in the southern area of the German Bight (Barth et al., 2010; Meyerjürgens et al., 2019; Port et al., 2011; Stanev, Ziemer, et al., 2015). At larger scales, the dispersion remains anisotropic but in contrast to the intermediate scales with higher magnitudes of meridional dispersion. At these scales, the drifters leave the area of the German Bight and are transported along the east coast of Denmark toward north. Figure 6 indicates that the amplitude of tidal currents decreases in the northern part of the German Bight, and the meridional velocity components along the Danish coast become more dominant. The transition of zonally dominated to meridionally dominated dispersion occurs in order of the regime transition from ballistic to Richardson dispersion. Thus, there is evidence that anisotropic changes contribute to regime transitions. A significant decrease in zonal dispersion is observed from 40 to 60 days for C_1. In this phase, the drifters reached the north coast of Denmark, entering the Skagerrak and were recirculated in the southern part of the Skagerrak. Recirculation of North Atlantic surface water induced by strong surface currents in this area was also found in a detailed study of the physical oceanography in the Skagerrak (Svendsen et al., 1996). The sharp decrease in zonal dispersion could be explained with a complex interaction of boundary effects caused by the bathymetry gradients and a complex current system which connects the North Sea with the Skagerrak. As a result, the drifters are recirculated due to the interaction of the water inflow of the North Sea and the outflowing water of the Baltic Sea. This effect was also highlighted by a recent study that discussed the propagation of virtual particles released in the North Sea (Gutow et al., 2018). After 60 days, a significant increase in zonal dispersion is observed for C_1. As a consequence, the drifters are distributed in different directions after being recirculated, which is indicated in the trajectories (Figure 1a).

4.3. Tidal Effects on Diffusivity

The influence of tides on relative diffusivity increases with growing pair separation. On the submesoscales, with separation scales up to 10 km, no significant peaks were observed in the FFTs. On these scales, the relative dispersion and diffusivity indicate a nonlocal dispersion regime influenced by processes affecting the dispersion with larger spatial scales then pair separation. Tidal forces have no significant contribution to the relative diffusivity on these scales. At larger separation scales, where local processes control drifter dispersion, the influence of semidiurnal tides is manifested by the FFTs. The interpretation of these results suggests that at small separation scales, the tidal motions of the drifters are correlated, and tides, therefore, do not contribute to the relative diffusivity. With increasing separation scales, tidal motions on drifter pairs are uncorrelated due to spatial variations and time delays of the tidal wave. Romero et al. (2013) simulated the particle pair dispersion in the Southern California Bight and found no significant contribution of tides on the particle dispersion in the submesoscales. Our results give an observational prove that the influence of tides on dispersion in shallow shelf seas depends on pair separation and becomes apparent in the mesoscales where tidal motions are not correlated.

Furthermore, the influence of shallow-water tidal constituents (M_4 and M_6) can be detected in the FFTs with maximum separations above 50 km. As demonstrated in the theoretical study of Stanev et al. (2016), shallow-water constituents have a significant influence on the tidal dynamics in the coastal areas of the German Bight and require an exact representation in coastal circulation models. Our results give an observational support to this modeling study demonstrating that shallow-water tides have a significant influence on diffusivities. Therefore, shallow-water tides need to be realistically included in numerical models for particle tracking. Also, Suanda et al. (2018) reported 3 to 4 times higher dispersion rates for particle simulation in the coastal area with baroclinic tides in comparison to simulation forced by barotropic tides. The interaction between barotropic tides and mesoscale processes was addressed in a recent study by Stanev and Ricker (2020). The results indicate that barotropic tides contribute massively to the transformation of wave number spectra of sea surface height, which become visible by the flattening of the spectrum, suggesting that high-frequency processes overshadow the quasi-geostrophic processes. Furthermore, the length of the simulated particle trajectories increases by approximately 40% under barotropic tidal forcing. However, the contribution of tides to the mesoscale diffusivity in Lagrangian particle tracking remains unclear and needs to be investigated by further studies.

4.4. Implications for Numerical Modeling

Increasing temporal resolution of the ocean general circulations models (OGCMs) output shows increasing relative diffusivities in modeled particle trajectories but still a weaker diffusivity than the values of real drifter trajectories (De Dominicis et al., 2012). One plausible explanation is that the temporal model resolution does not fully resolve tidal currents, especially the semidiurnal components, which leads to underestimated diffusivities (De Dominicis et al., 2012; Döös et al., 2011). The temporal resolution is also particularly important for the representation of overtides with periods of several hours, which also contribute to the diffusivity. Since the effects of tidal-induced diffusivities become significantly apparent on separation scales above 50 km, the trajectory length of simulated or observed drifters should cover time scales of at least 35 days to investigate mesoscale diffusivities. Our observations suggest that at these temporal scales, the influence of tides on diffusivities is significant due to the uncorrelated tidal motions. De Dominicis et al. (2012) divided the trajectories into subsegments of 1, 4, and 7 days to estimate diffusivities from drifter observations. This method may underestimate scale-dependent diffusivities occurring at separation scales of more than 50 km.

Our results show that analyzed semidiurnal and shallow water tidal constituents (M_2, M_4, and M_6) induce a relative diffusivity of 289.5 $m^2\ s^{-1}$, which is around 27% of the total estimated relative diffusivity at separation scales of 150 km. The scale dependence of the dispersion properties has also been reported on the submesoscales in the Santa Barbara Channel (Ohlmann et al., 2012). This study indicated that observed and modeled dispersion values show the best agreement by a scale-dependent parametrization of the relative velocity of particle pairs. They reported values of 0.7 and 5.1 cm s^{-1} (corresponding to diffusivities of 0.5 and 28 $m^2\ s^{-1}$) for separation scales of 5 m and 2 km, respectively. Our results show scale-dependent diffusivities, which are about 10 times higher for the mesoscales with separation scales up to 150 km, in comparison to the results observed by Ohlmann et al. (2012) on the submesoscales. Thus, we suggest analyzing the relative diffusivity of simulated particles with and without barotropic tidal forcing with different spatial and

temporal resolutions in OGCMs to compare the results to the findings of our study. One step in this direction was presented by Stanev and Ricker (2020).

Besides, alternative diffusivity parameterizations should be considered and tested, which include scale-dependent effects. New parameterization concepts were presented by Cushman-Roisin (2008) and Kämpf and Cox (2016) in which the diffusivity depends on the separation of the particles. The results of our study provide observational evidence that the implementation of scale-dependent diffusivity parameterizations in appropriate lateral and temporal resolved models can be a crucial step forward to improve the diffusivity in OGCMs and the prediction of Lagrangian particles in tidally influenced shelf seas. An improved representation of diffusivities is necessary to predict the dispersion of oil spills accurately, pollutants and biological substances in tidally influenced shelf seas (Lynge et al., 2010; Mantovanelli et al., 2012; Ohlmann & Mitarai, 2010; Suanda et al., 2018).

5. Summary and Conclusions

The description of the turbulent flow field via statistical Lagrangian metrics derived from in situ observations is fundamental for the accurate parameterization and validation of numerical modeling frameworks. This study provides the first description of the turbulent flow field on different spatial scales in the North Sea derived from Lagrangian observations. Drifter dispersion of both clusters shows evidence of a decreasing trend in the vicinity of a tidal mixing front followed by exponential dispersion at the submesoscales. At intermediate scales, dispersion scales as ballistic, followed by a Richardson regime. The analysis of the diffusivities is consistent with these findings, but the results of the FSLEs contradict the results of dispersion and diffusivities at small scales and large scales for C_1. Discrepancies of different statistical Lagrangian metrics derived from drifter observations are not uncommon and were also observed in other ocean areas. Overall, the analyses of the different Lagrangian metrics suggest that tracer stirring is nonlocal at the submesoscales and become local at separation scales larger than 10 km.

The e-folding times indicate strong increasing dispersion at the submesoscales and the analysis of zonal and meridional components showing isotropic behavior. At the mesoscales, dispersion appear to be anisotropic with higher magnitudes of zonal dispersion. In the area of the Skagerrak, the dispersion remains anisotropic but with higher magnitudes of meridional dispersion.

Furthermore, we provide, to our knowledge, the first analysis on the relative diffusivity at different spatial scales derived from pairwise deployed drifters in a highly tidally influenced shelf sea. Our results show a scale-dependent effect on diffusivities due to tidal effects, which increase at growing separation scales. By analyzing the FFTs of the relative diffusivities, we show that the influence of tides on the relative diffusivities becomes significantly apparent for drifter separations above 50 km, reaching 27% of the total diffusivity at separations scales of 150 km.

Since the diffusion of particles in numerical frameworks is often implicit, represented by the large-scale straining of the velocity field, the question arises on how the particle tracking models in tidally influenced shelf seas perform in comparison to our observations. The results of this study indicate that numerical models should incorporate realistic representations of tidal effects and consider testing scale-dependent diffusivity parameterizations.

Acknowledgments

This work was carried out within the project Macroplastics Pollution in the southern North Sea—Sources, Pathways and Abatement Strategies (Grant ZN3176) funded by the German Federal State of Lower Saxony. We thank Axel Braun, Andreas Sommer, Michael Butter, Elisa Schöpe, and Lars Meyer-Hagg for the support in constructing the drifters. We thank the master and crew onboard the RV Heincke HE520 for supporting the drifter deployments. We want to thank Oliver Zielinski and Ulrike Feudel for inspiring discussions and providing important comments. We would like to thank the editor Nadia Pinardi and two anonymous reviewers for their constructive comments, which helped to improve this paper.

Data Availability Statement

Drifter trajectories are available at the PANGEA database (https://doi.org/10.1594/PANGAEA.910175). Sea surface temperature data are produced by the Group for High Resolution Sea Surface Temperature (GHRSST) Multi-scale Ultra-high Resolution (MUR). SST data (CMEMS-SST-PUM-010-010-025) were obtained from the NASA EOSDIS Physical Oceanography Distributed Active Archive Center (PO.DAAC) at the Jet Propulsion Laboratory, Pasadena, CA (https://doi.org/10.5067/GHGMR-4FJ01).

References

Acha, E. M., Mianzan, H. W., Iribarne, O., Gagliardini, D. A., Lasta, C., & Daleo, P. (2003). The role of the Río de la Plata bottom salinity front in accumulating debris. *Marine Pollution Bulletin*, *46*(2), 197–202. https://doi.org/10.1016/S0025-326X(02)00356-9

Artale, V., Boffetta, G., Celani, A., Cencini, M., & Vulpiani, A. (1997). Dispersion of passive tracers in closed basins: Beyond the diffusion coefficient. *Physics of Fluids*, *9*(11), 3162–3171. https://doi.org/10.1063/1.869433

Aurell, E., Boffetta, G., Crisanti, A., Paladin, G., & Vulpiani, A. (1997). Predictability in the large: An extension of the concept of Lyapunov exponent. *Journal of Physics A: Mathematical and General*, *30*(1), 1–26. https://doi.org/10.1088/0305-4470/30/1/003

Badin, G., Tandon, A., & Mahadevan, A. (2011). Lateral mixing in the pycnocline by baroclinic mixed layer eddies. *Journal of Physical Oceanography*, *41*(11), 2080–2101. https://doi.org/10.1175/JPO-D-11-05.1

Badin, G., Williams, R. G., Holt, J. T., & Fernand, L. J. (2009). Are mesoscale eddies in shelf seas formed by baroclinic instability of tidal fronts? *Journal of Geophysical Research*, *114*, C10021. https://doi.org/10.1029/2009JC005340

Barth, A., Alvera-Azcárate, A., Gurgel, K.-W., Staneva, J., Port, A., Beckers, J.-M., & Stanev, E. V. (2010). Ensemble perturbation smoother for optimizing tidal boundary conditions by assimilation of high-frequency radar surface currents—Application to the German Bight. *Ocean Science*, *6*(1), 161–178. https://doi.org/10.5194/os-6-161-2010

Baschek, B., Schroeder, F., Brix, H., Riethmüller, R., Badewien, T. H., Breitbach, G., et al. (2017). The Coastal Observing System for Northern and Arctic Seas (COSYNA). *Ocean Science*, *13*(3), 379–410. https://doi.org/10.5194/os-13-379-2017

Becker, G. A., Dick, S., & Dippner, J. W. (1992). Hydrography of the German Bight. *Marine Ecology Progress Series*, *91*, 9–18. http://doi.org/10.3354/meps091009

Becker, G. A., Giese, H., Isert, K., König, P., Langenberg, H., Pohlmann, T., & Schrum, C. (1999). Mesoscale structures, fluxes and water mass variability in the German Bight as exemplified in the KUSTOS—Experiments and numerical models. *Deutsche Hydrographische Zeitschrift*, *51*(2-3), 155–179. https://doi.org/10.1007/BF02764173

Bennett, A. (2006). *Lagrangian fluid dynamics*. Cambridge: Cambridge University Press. https://doi.org/10.1017/CBO9780511734939

Beron-Vera, F. J., & LaCasce, J. H. (2016). Statistics of simulated and observed pair separations in the Gulf of Mexico. *Journal of Physical Oceanography*, *46*(7), 2183–2199. https://doi.org/10.1175/JPO-D-15-0127.1

Berti, S., Santos, F. A. D., Lacorata, G., & Vulpiani, A. (2011). Lagrangian drifter dispersion in the southwestern Atlantic Ocean. *Journal of Physical Oceanography*, *41*(9), 1659–1672. https://doi.org/10.1175/2011JPO4541.1

Callies, U., Carrasco, R., Floeter, J., Horstmann, J., & Quante, M. (2019). Submesoscale dispersion of surface drifters in a coastal sea near offshore wind farms. *Ocean Science*, *15*(4), 865–889. https://doi.org/10.5194/os-15-865-2019

Cencini, M., & Vulpiani, A. (2013). Finite size Lyapunov exponent: Review on applications. *Journal of Physics A: Mathematical and Theoretical*, *46*, 254019. https://doi.org/10.1088/1751-8113/46/25/254019

Christensen, K., Breivik, Ø., Dagestad, K.-F., Röhrs, J., & Ward, B. (2018). Short-term predictions of oceanic drift. *Oceanography*, *31*(3), 59–67. https://doi.org/10.5670/oceanog.2018.310

Codiga, D. L. (2011). Unified tidal analysis and prediction using the UTide Matlab functions. https://doi.org/10.13140/rg.2.1.3761.2008

Corrado, R., Lacorata, G., Palatella, L., Santoleri, R., & Zambianchi, E. (2017). General characteristics of relative dispersion in the ocean. *Scientific Reports*, *7*(1), 46,291. https://doi.org/10.1038/srep46291

Critchell, K., Grech, A., Schlaefer, J., Andutta, F. P., Lambrechts, J., Wolanski, E., & Hamann, M. (2015). Modelling the fate of marine debris along a complex shoreline: Lessons from the Great Barrier Reef. *Estuarine, Coastal and Shelf Science*, *167*, 414–426. https://doi.org/10.1016/j.ecss.2015.10.018

Cushman-Roisin, B. (2008). Beyond eddy diffusivity: An alternative model for turbulent dispersion. *Environmental Fluid Mechanics*, *8*(5-6), 543–549. https://doi.org/10.1007/s10652-008-9082-7

D'Asaro, E. A., Shcherbina, A. Y., Klymak, J. M., Molemaker, J., Novelli, G., Guigand, C. M., et al. (2018). Ocean convergence and the dispersion of flotsam. *Proceedings of the National Academy of Sciences*, *115*(6), 1162–1167. https://doi.org/10.1073/pnas.1718453115

De Dominicis, M., Bruciaferri, D., Gerin, R., Pinardi, N., Poulain, P. M., Garreau, P., et al. (2016). A multi-model assessment of the impact of currents, waves and wind in modelling surface drifters and oil spill. *Deep-Sea Research Part II: Topical Studies in Oceanography*, *133*, 21–38. https://doi.org/10.1016/j.dsr2.2016.04.002

De Dominicis, M., Leuzzi, G., Monti, P., Pinardi, N., & Poulain, P.-M. (2012). Eddy diffusivity derived from drifter data for dispersion model applications. *Ocean Dynamics*, *62*(9), 1381–1398. https://doi.org/10.1007/s10236-012-0564-2

Delandmeter, P., Lambrechts, J., Marmorino, G. O., Legat, V., Wolanski, E., Remacle, J.-F., et al. (2017). Submesoscale tidal eddies in the wake of coral islands and reefs: Satellite data and numerical modelling. *Ocean Dynamics*, *67*(7), 897–913. https://doi.org/10.1007/s10236-017-1066-z

Dippner, J. W. (1993). A frontal-resolving model for the German Bight. *Continental Shelf Research*, *13*(1), 49–66. https://doi.org/10.1016/0278-4343(93)90035-V

Döös, K., Rupolo, V., & Brodeau, L. (2011). Dispersion of surface drifters and model-simulated trajectories. *Ocean Modelling*, *39*(3-4), 301–310. https://doi.org/10.1016/j.ocemod.2011.05.005

Dräger-Dietel, J., Jochumsen, K., Griesel, A., & Badin, G. (2018). Relative dispersion of surface drifters in the Benguela upwelling region. *Journal of Physical Oceanography*, *48*(10), 2325–2341. https://doi.org/10.1175/JPO-D-18-0027.1

Drinkwater, K. F., & Loder, J. W. (2001). Near-surface horizontal convergence and dispersion near the tidal-mixing front on northeastern Georges Bank. *Deep Sea Research Part II: Topical Studies in Oceanography*, *48*(1–3), 311–339. https://doi.org/10.1016/S0967-0645(00)00084-9

Essink, S., Hormann, V., Centurioni, L. R., & Mahadevan, A. (2019). Can we detect submesoscale motions in drifter pair dispersion? *Journal of Physical Oceanography*, *49*(9), 2237–2254. https://doi.org/10.1175/JPO-D-18-0181.1

Fritsch, F. N., & Carlson, R. E. (1980). Monotone piecewise cubic interpolation. *SIAM Journal on Numerical Analysis*, *17*(2), 238–246. https://doi.org/10.1137/0717021

Gawarkiewicz, G., Monismith, S., & Largier, J. (2007). Observing larval transport processes affecting population connectivity: Progress and challenges. *Oceanography*, *20*(3), 40–53. https://doi.org/10.5670/oceanog.2007.28

Graham, J. A., O'Dea, E., Holt, J., Polton, J., Hewitt, H. T., Furner, R., et al. (2018). AMM15: A new high-resolution NEMO configuration for operational simulation of the European north-west shelf. *Geoscientific Model Development*, *11*(2), 681–696. https://doi.org/10.5194/gmd-11-681-2018

Guihou, K., Polton, J., Harle, J., Wakelin, S., O'Dea, E., & Holt, J. (2018). Kilometric scale modeling of the north west European shelf seas: Exploring the spatial and temporal variability of internal tides: Modeling of the Atlantic European shelf. *Journal of Geophysical Research: Oceans*, *123*, 688–707. https://doi.org/10.1002/2017JC012960

Gutow, L., Ricker, M., Holstein, J. M., Dannheim, J., Stanev, E. V., & Wolff, J.-O. (2018). Distribution and trajectories of floating and benthic marine macrolitter in the south-eastern North Sea. *Marine Pollution Bulletin*, *131*(Pt A), 763–772. https://doi.org/10.1016/j.marpolbul.2018.05.003

Haller, G., & Yuan, G. (2000). Lagrangian coherent structures and mixing in two-dimensional turbulence. *Phys. Nonlinear Phenom.*, *147*(3-4), 352–370. https://doi.org/10.1016/S0167-2789(00)00142-1

Haza, A. C., Griffa, A., Martin, P., Molcard, A., Özgökmen, T. M., Poje, A. C., et al. (2007). Model-based directed drifter launches in the Adriatic Sea: Results from the DART experiment. *Geophysical Research Letters*, *34*, L10605. https://doi.org/10.1029/2007GL029634

Haza, A. C., Özgökmen, T. M., Griffa, A., Poje, A. C., & Lelong, M.-P. (2014). How does drifter position uncertainty Affect Ocean dispersion estimates? *Journal of Atmospheric and Oceanic Technology*, *31*(12), 2809–2828. https://doi.org/10.1175/JTECH-D-14-00107.1

Haza, A. C., Poje, A. C., Özgökmen, T. M., & Martin, P. (2008). Relative dispersion from a high-resolution coastal model of the Adriatic Sea. *Ocean Modelling*, *22*(1-2), 48–65. https://doi.org/10.1016/j.ocemod.2008.01.006

Hinojosa, I. A., Pizarro, M., Ramos, M., & Thiel, M. (2010). Spatial and temporal distribution of floating kelp in the channels and fjords of southern Chile. *Estuarine, Coastal and Shelf Science*, *87*(3), 367–377. https://doi.org/10.1016/j.ecss.2009.12.010

Huthnance, J. (1991). Physical oceanography of the North Sea. *Ocean and Shoreline Management*, *16*(3-4), 199–231. https://doi.org/10.1016/0951-8312(91)90005-M

Kämpf, J., & Cox, D. (2016). Towards improved numerical schemes of turbulent lateral dispersion. *Ocean Modelling*, *106*, 1–11. https://doi.org/10.1016/j.ocemod.2016.08.003

Klein, P., & Lapeyre, G. (2009). The oceanic vertical pump induced by mesoscale and submesoscale turbulence. *Annual Review of Marine Science*, *1*(1), 351–375. https://doi.org/10.1146/annurev.marine.010908.163704

Koszalka, I., LaCasce, J. H., & Orvik, K. A. (2009). Relative dispersion in the Nordic Seas. *Journal of Marine Research*, *67*(4), 411–433. https://doi.org/10.1357/002224009790741102

LaCasce, J. H. (2010). Relative displacement probability distribution functions from balloons and drifters. *Journal of Marine Research*, *68*(3), 433–457. https://doi.org/10.1357/002224010794657155

LaCasce, J. H., & Ohlmann, C. (2003). Relative dispersion at the surface of the Gulf of Mexico. *Journal of Marine Research*, *61*(3), 285–312. https://doi.org/10.1357/002224003322201205

Lacorata, G., Aurell, E., & Vulpiani, A. (2001). Drifter dispersion in the Adriatic Sea: Lagrangian data and chaotic model. *Annales de Geophysique*, *19*(1), 121–129. https://doi.org/10.5194/angeo-19-121-2001

Langenberg, H. (1998). Features of coastal current instabilities in the North Sea: Results of a numerical model. *Journal of Geophysical Research*, *103*(C4), 7681–7691. https://doi.org/10.1029/98JC00100

Laxague, N. J. M., Özgökmen, T. M., Haus, B. K., Novelli, G., Shcherbina, A., Sutherland, P., et al. (2018). Observations of near-surface current shear help describe oceanic oil and plastic transport: Very near surface current shear. *Geophysical Research Letters*, *45*, 245–249. https://doi.org/10.1002/2017GL075891

Lévy, M., Ferrari, R., Franks, P. J. S., Martin, A. P., & Rivière, P. (2012). Bringing physics to life at the submesoscale: Frontier. *Geophysical Research Letters*, *39*, L14602. https://doi.org/10.1029/2012GL052756

Lui, H., Shah, S., & Jiang, W. (2004). On-line outlier detection and data cleaning. *Computers & Chemical Engineering*, *28*(9), 1635–1647. https://doi.org/10.1016/j.compchemeng.2004.01.009

Lumpkin, R., & Elipot, S. (2010). Surface drifter pair spreading in the North Atlantic. *Journal of Geophysical Research*, *115*, C12017. https://doi.org/10.1029/2010JC006338

Lumpkin, R., Özgökmen, T., & Centurioni, L. (2017). Advances in the application of surface drifters. *Annual Review of Marine Science*, *9*(1), 59–81. https://doi.org/10.1146/annurev-marine-010816-060641

Lynge, B. K., Berntsen, J., & Gjevik, B. (2010). Numerical studies of dispersion due to tidal flow through Moskstraumen, northern Norway. *Ocean Dynamics*, *60*(4), 907–920. https://doi.org/10.1007/s10236-010-0309-z

Mantovanelli, A., Heron, M. L., Heron, S. F., & Steinberg, C. R. (2012). Relative dispersion of surface drifters in a barrier reef region: Drifter dispersion in the GBR. *Journal of Geophysical Research*, *117*, C11016. https://doi.org/10.1029/2012JC008106

Maximenko, N., Hafner, J., & Niiler, P. (2012). Pathways of marine debris derived from trajectories of Lagrangian drifters. *Marine Pollution Bulletin*, *65*(1-3), 51–62. https://doi.org/10.1016/j.marpolbul.2011.04.016

McWilliams, J. C. (2016). Submesoscale currents in the ocean. *Proceedings of the Royal Society a Mathematical, Physical and Engineering Sciences*, *472*, 20160117. https://doi.org/10.1098/rspa.2016.0117

Merlivat, L., Boutin, J., & Antoine, D. (2015). Roles of biological and physical processes in driving seasonal air-sea CO_2 flux in the Southern Ocean: New insights from CARIOCA pCO_2. *Journal of Marine Systems*, *147*, 9–20. https://doi.org/10.1016/j.jmarsys.2014.04.015

Meyerjürgens, J., Badewien, T. H., Garaba, S. P., Wolff, J.-O., & Zielinski, O. (2019). A state-of-the-art compact surface drifter reveals pathways of floating marine litter in the German Bight. *Frontiers in Marine Science*, *6*. https://doi.org/10.3389/fmars.2019.00058

Ohlmann, J. C., LaCasce, J. H., Washburn, L., Mariano, A. J., & Emery, B. (2012). Relative dispersion observations and trajectory modeling in the Santa Barbara Channel: Lagrangian statistics and modeling. *Journal Geophysical Research: Oceans*, *117*(C5), C05040. https://doi.org/10.1029/2011JC007810

Ohlmann, J. C., & Mitarai, S. (2010). Lagrangian assessment of simulated surface current dispersion in the coastal ocean: Lagrangian model assessment. *Geophysical Research Letters*, *37*, L17602. https://doi.org/10.1029/2010GL044436

Ollitrault, M., Gabillet, C., & De Verdière, A. C. (2005). Open ocean regimes of relative dispersion. *Journal of Fluid Mechanics*, *533*, 381–407. https://doi.org/10.1017/S0022112005004556

Orre, S., Gjevik, B., & LaCasce, J. H. (2006). Characterizing chaotic dispersion in a coastal tidal model. *Continental Shelf Research*, *26*(12-13), 1360–1374. https://doi.org/10.1016/j.csr.2005.11.015

Otto, L., Zimmerman, J. T. F., Furnes, G. K., Mork, M., Saetre, R., & Becker, G. (1990). Review of the physical oceanography of the North Sea. *Netherlands Journal of Sea Research*, *26*(2-4), 161–238. https://doi.org/10.1016/0077-7579(90)90091-T

Özgökmen, T. M., Poje, A. C., Fischer, P. F., Childs, H., Krishnan, H., Garth, C., et al. (2012). On multi-scale dispersion under the influence of surface mixed layer instabilities and deep flows. *Ocean Modelling*, *56*, 16–30. https://doi.org/10.1016/j.ocemod.2012.07.004

Poje, A. C., Özgökmen, T. M., Bogucki, D. J., & Kirwan, A. D. (2017). Evidence of a forward energy cascade and Kolmogorov self-similarity in submesoscale ocean surface drifter observations. *Physics of Fluids*, *29*, 020701. https://doi.org/10.1063/1.4974331

Poje, A. C., Ozgokmen, T. M., Lipphardt, B. L., Haus, B. K., Ryan, E. H., Haza, A. C., et al. (2014). Submesoscale dispersion in the vicinity of the Deepwater Horizon spill. *Proceedings of the National Academy of Sciences*, *111*(35), 12,693–12,698. https://doi.org/10.1073/pnas.1402452111

Port, A., Gurgel, K.-W., Staneva, J., Schulz-Stellenfleth, J., & Stanev, E. V. (2011). Tidal and wind-driven surface currents in the German Bight: HFR observations versus model simulations. *Ocean Dynamics*, *61*(10), 1567–1585. https://doi.org/10.1007/s10236-011-0412-9

Poulain, P.-M., Gerin, R., Mauri, E., & Pennel, R. (2009). Wind effects on drogued and undrogued drifters in the eastern Mediterranean. *Journal of Atmospheric and Oceanic Technology*, *26*(6), 1144–1156. https://doi.org/10.1175/2008JTECHO618.1

Richardson, L. F. (1926). Atmospheric diffusion shown on a distance-neighbour graph. *Proceedings of the Royal Society a Mathematical, Physical and Engineering Sciences*, *110*(756), 709–737. https://doi.org/10.1098/rspa.1926.0043

Roach, C. J., Balwada, D., & Speer, K. (2018). Global observations of horizontal mixing from Argo float and surface drifter trajectories. *Journal of Geophysical Research: Oceans*, *123*, 4560–4575. https://doi.org/10.1029/2018JC013750

Romero, L., Uchiyama, Y., Ohlmann, J. C., McWilliams, J. C., & Siegel, D. A. (2013). Simulations of nearshore particle-pair dispersion in Southern California. *Journal of Physical Oceanography*, *43*(9), 1862–1879. https://doi.org/10.1175/JPO-D-13-011.1

Sansón, L. Z., Pérez-Brunius, P., & Sheinbaum, J. (2017). Surface relative dispersion in the southwestern Gulf of Mexico. *Journal of Physical Oceanography*, *47*(2), 387–403. https://doi.org/10.1175/JPO-D-16-0105.1

Schroeder, K., Chiggiato, J., Haza, A. C., Griffa, A., Özgökmen, T. M., Zanasca, P., et al. (2012). Targeted Lagrangian sampling of submesoscale dispersion at a coastal frontal zone: LIDEX10-REP10. *Geophysical Research Letters*, *39*, L11608. https://doi.org/10.1029/2012GL051879

Skov, H., & Prins, E. (2001). Impact of estuarine fronts on the dispersal of piscivorous birds in the German Bight. *Marine Ecology Progress Series*, *214*, 279–287. https://doi.org/10.3354/meps214279

Spydell, M., Feddersen, F., Guza, R. T., & Schmidt, W. E. (2007). Observing surf-zone dispersion with drifters. *Journal of Physical Oceanography*, *37*(12), 2920–2939. https://doi.org/10.1175/2007JPO3580.1

Spydell, M. S., Feddersen, F., Olabarrieta, M., Chen, J., Guza, R. T., Raubenheimer, B., & Elgar, S. (2015). Observed and modeled drifters at a tidal inlet: Drifters at the new river inlet. *Journal of Geophysical Research: Oceans*, *120*, 4825–4844. https://doi.org/10.1002/2014JC010541

Stanev, E. V., Badewien, T. H., Freund, H., Grayek, S., Hahner, F., Meyerjürgens, J., et al. (2019). Extreme westward surface drift in the North Sea: Public reports of stranded drifters and Lagrangian tracking. *Continental Shelf Research*, *177*, 24–32. https://doi.org/10.1016/j.csr.2019.03.003

Stanev, E. V., & Ricker, M. (2020). Interactions between barotropic tides and mesoscale processes in deep ocean and shelf regions. *Ocean Dynamics*, *70*(5), 713–728. https://doi.org/10.1007/s10236-020-01348-6

Stanev, E. V., Schulz-Stellenfleth, J., Staneva, J., Grayek, S., Grashorn, S., Behrens, A., et al. (2016). Ocean forecasting for the German Bight: From regional to coastal scales. *Ocean Science*, *12*(5), 1105–1136. https://doi.org/10.5194/os-12-1105-2016

Stanev, E. V., Ziemer, F., Schulz-Stellenfleth, J., Seemann, J., Staneva, J., & Gurgel, K.-W. (2015). Blending surface currents from HF radar observations and numerical modeling: Tidal hindcasts and forecasts. *Journal of Atmospheric and Oceanic Technology*, *32*, 256–281. https://doi.org/10.1175/JTECH-D-13-00164.1

Stanev, E. V., Al-Nadhairi, R., & Valle-Levinson, A. (2015). The role of density gradients on tidal asymmetries in the German Bight. *Ocean Dynamics*, *65*(1), 77–92. https://doi.org/10.1007/s10236-014-0784-8

Suanda, S. H., Feddersen, F., & Kumar, N. (2017). The effect of barotropic and baroclinic tides on coastal stratification and mixing. *Journal of Geophysical Research: Oceans*, *122*, 10,156–10,173. https://doi.org/10.1002/2017JC013379

Suanda, S. H., Feddersen, F., Spydell, M. S., & Kumar, N. (2018). The effect of barotropic and baroclinic tides on three-dimensional coastal dispersion. *Geophysical Research Letters*, *45*, 11,235–11,246. https://doi.org/10.1029/2018GL079884

Svendsen, E., Bemtsen, J., Skogen, M., Ådlandsvik, B., & Martinsen, E. (1996). Model simulation of the Skagerrak circulation and hydrography during Skagex. *Journal of Marine Systems*, *8*(3-4), 219–236. https://doi.org/10.1016/0924-7963(96)00007-3

Thiel, M., Hinojosa, I. A., Joschko, T., & Gutow, L. (2011). Spatio-temporal distribution of floating objects in the German Bight (North Sea). *Journal of Sea Research*, *65*(3), 368–379. https://doi.org/10.1016/j.seares.2011.03.002

Tseng, R.-S. (2002). On the dispersion and diffusion near estuaries and around islands. *Estuarine, Coastal and Shelf Science*, *54*(1), 89–100. https://doi.org/10.1006/ecss.2001.0830

van Sebille, E., Waterman, S., Barthel, A., Lumpkin, R., Keating, S. R., Fogwill, C., & Turney, C. (2015). Pairwise surface drifter separation in the western Pacific sector of the Southern Ocean: Southern Ocean drifter dispersion. *Journal of Geophysical Research: Oceans*, *120*, 6769–6781. https://doi.org/10.1002/2015JC010972